Cooling to the Ground State of Axial Motion
for One Atom Strongly Coupled to an Optical Cavity

A. D. Boozer, A. Boca, R. Miller, T. E. Northup, and H. J. Kimble

Norman Bridge Laboratory of Physics 12-33
California Institute of Technology, Pasadena, CA 91125
(Dated: August 4, 2018)

Localization to the ground state of axial motion is demonstrated for a single, trapped atom strongly coupled to the field of a high finesse optical resonator. The axial atomic motion is cooled by way of coherent Raman transitions on the red vibrational sideband. An efficient state detection scheme enabled by strong coupling in cavity QED is used to record the Raman spectrum, from which the state of atomic motion is inferred. We find that the lowest vibrational level of the axial potential with zero-point energy $\hbar\omega_a/2k_B = 13$ μK is occupied with probability $P_0 \simeq 0.95$.

Single atoms strongly coupled to the fields of high quality optical resonators are of fundamental importance in Quantum Optics and, more generally, can be used for many tasks in quantum information science, including the implementation of scalable quantum computation [1, 2] and the realization of distributed quantum networks [3, 4]. In recent years, significant experimental progress to develop tools suitable for these tasks has been made by employing optical forces to localize individual atoms within optical cavities in a regime of strong coupling [5, 6, 7, 8, 9, 10, 11], as well as by combining trapped ions with optical cavities [12]. Scientific advances thereby enabled include the observation of the vacuum-Rabi spectrum for an individual atom [9] and vacuum-stimulated cooling [10].

Although great strides are thus being made with atoms localized and strongly coupled to the fields of optical cavities [13], it has not previously been possible to access the quantum regime for the atomic center-of-mass motion in cavity QED. Qualitatively new phenomena have been predicted in this regime for which a quantized treatment is required for both the internal (i.e., the atomic dipole and cavity field) and external (i.e., atomic motion) degrees of freedom, as was first recognized in the seminal work in Refs. [15, 16, 17] and in the years since [18, 19, 20, 21, 22, 23, 24]. Examples include the exploitation of strong coupling for the reliable transfer of quantized states of atomic motion to quantum states of light, and conversely [24], as well as for measurements that surpass the standard quantum limit for sensing atomic position [18].

Our effort towards quantum control of atomic motion in cavity QED unabashedly follows the remarkable set of achievements for trapped ions [25] and atoms in optical lattices [26], for which such control has led to the creation of manifestly quantum (i.e., nonclassical) states of motion and to the manipulation of quantum information. A first, enabling step in many of these investigations has been the capability to cool to the ground state of motion for single trapped atoms or ions.

In this Letter we report localization to the ground state of motion for one atom trapped in an optical cavity in a
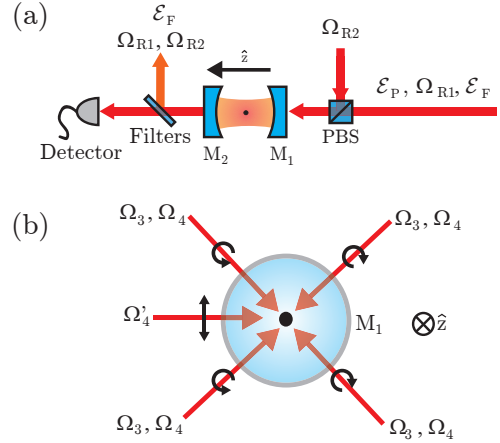

FIG. 1: Schematic of the experiment. The cavity is represented (a) from the side and (b) along its axis. Shown are the various beams used in the experiment: linearly polarized probe $\mathcal{E}_p$, FORT $\mathcal{E}_F$, pumping Ω'_4, and Raman beams $\Omega_{R1,R2}$, as well as the circularly polarized lattice beams $\Omega_{3,4}$.

regime of strong coupling [11]. Resolved sideband cooling to the ground state is accomplished with a coherent pair of intracavity Raman fields. To deduce the resulting state of atomic motion, we introduce a new scheme for recording Raman spectra by way of the strong interaction of the atom with a resonant cavity probe. Our scheme is the cavity QED equivalent of state detection in free space by quantum-jump spectroscopy [25], and achieves a confidence level for state discrimination $> 98\%$ in 100 μs. From the Raman spectra, we infer that the lowest vibrational level $n = 0$ of the axial potential is occupied with probability $P_0 \simeq 0.95$ for one trapped atom.

A schematic of the experimental setup is given in Fig. 1. At the heart of the system is the Fabry-Perot cavity formed by mirrors (M_1, M_2). The cavity length is stabilized to $l_0 = 42.2$ μm using an independent locking laser, such that a TEM_{00} mode is resonant with the $6S_{1/2}, F = 4 \rightarrow 6P_{3/2}, F' = 5'$ transition of the $D2$ line in Cs. The resulting atom-cavity coupling gives a maximum single-photon Rabi frequency of $2g_0/2\pi = 68$ MHz

for $(F = 4, m_F = \pm 4) \to (F' = 5', m'_F = \pm 5)$. The decay rates are $\gamma/2\pi = 2.6$ MHz for the $6P_{3/2}$ excited states, and $\kappa/2\pi = 4.1$ MHz for the cavity field. Because $g_0 \gg (\gamma, \kappa)$, our system is in the strong coupling regime of cavity QED [11], with critical photon and atom numbers $n_0 \equiv \gamma^2/(2g_0^2) \approx 0.0029$ and $N_0 \equiv 2\kappa\gamma/g_0^2 \approx 0.018$.

Atoms are trapped by an intracavity far-off-resonant trap (FORT) at $\lambda_F = 935.6$ nm, which is driven by a linearly polarized input field $\mathcal{E}_F$ and is resonant with a TEM_{00} mode of the cavity with linewidth $\kappa_F/2\pi = 0.8$ GHz. At λ_F, states in the ground $F = 3, 4$ and excited state $F' = 5'$ manifolds experience nearly-equal trapping potentials. For states in the $F = 3, 4$ manifolds, this potential is independent of m_F and has a peak value of $U_F/h = -41$ MHz, while for states in the $F' = 5'$ manifold it has a weak dependence on m'_F [6, 9]. The standing-wave structure of the FORT forms independent wells where atoms may be trapped. Near the bottom of a FORT well the potential is approximately harmonic, with vibrational frequencies $\omega_a/2\pi = 530$ kHz for axial motion and $\omega_r/2\pi = 4.5$ kHz for radial motion.

To load atoms into the FORT, we release a cloud of cold atoms located ~ 3 mm above the cavity [6]. As the atoms fall through the cavity, we apply 5 ms of Ω_3, Ω_4 light by way of two pairs of counterpropagating $\sigma_+ - \sigma_-$ polarized beams, as illustrated in Fig. 1(b). These beams are blue detuned by $+10$ MHz from the $F = 3 \to F' = 3'$ and $F = 4 \to F' = 4'$ transitions, and cool the falling atoms via polarization gradient cooling [27]. We adjust the powers [28] of these beams so that the probability of loading at least one atom is ~ 0.3 per cloud drop.

Raman coupling between the $F = 3$ and $F = 4$ manifolds is generated by driving a cavity mode at $\lambda_R = 945.6$ nm with a pair of beams $\Omega_{R1,R2}$ that are phase-locked, lin $\perp$ lin polarized, and have a relative detuning $\omega_{R1} - \omega_{R2} = \Delta'_{HF} + \delta_R$, where $\Delta'_{HF}/2\pi = 9.19261$ GHz is the Cs hyperfine splitting [29] and δ_R is the Raman detuning. This cavity mode has a linewidth $\kappa_R/2\pi = 6$ GHz , and the Raman beams are tuned such that $\Omega_{R1(R2)}$ lies $\Delta'_{HF}/2$ above (below) cavity resonance. Since $\Omega_{R1,R2}$ drive a different mode of the cavity than $\mathcal{E}_F$, atoms trapped in different FORT wells see different Raman powers. If the relative spatial phase of the FORT and the Raman pair at the bottom of a given well is α, then an atom at this potential minimum sees a Raman power proportional to $\cos^2 \alpha$.

We typically set the optical power transmitted on resonance through the cavity for $\Omega_{R1,R2}$ to $P_{R1} = P_{R2} = 140$ μW, which gives a Rabi frequency [30] $\Omega_0/2\pi = 200$ kHz for atoms with $\alpha = 0$. The ac-Stark shift due to these Raman beams adds a correction to the FORT potential of $U_R/2\pi = 0.84$ MHz. To avoid heating the atom by switching U_R, we leave $\Omega_{R1,R2}$ on all the time, but usually keep them far-detuned ($\delta_R/2\pi = 85$ MHz) from Raman resonance. To drive Raman transitions, we change ω_{R2} so as to bring the pair into Raman resonance, whereas to fine-tune δ_R we vary ω_{R1}.

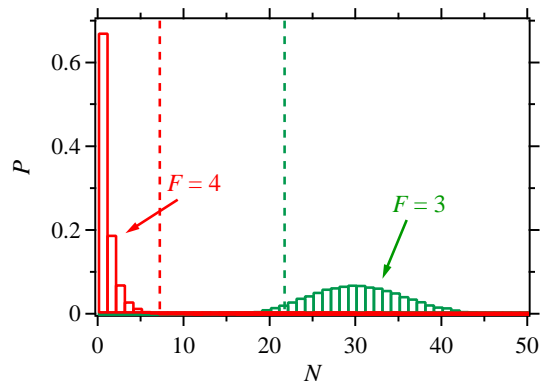Because the intensity of the Raman pair is spatially

FIG. 2: Histogram of counts recorded during 100 μs probing intervals for $N_e = 30$. The red (green) curve is the probability P of detecting a given number of counts N for an atom prepared in the $F = 4$ ($F = 3$) state. The dashed vertical bars indicate detection thresholds at $N = 0.25N_e$ and $N = 0.75N_e$.

varying, the Raman coupling can connect states with different vibrational quantum numbers. The form of this motional coupling is simple for atoms near the bottom of a FORT well where the axial and radial motions decouple, allowing us to consider the effect of the Raman coupling on the axial motion alone. In this harmonic limit, we can define a set of Fock states $\{|n\rangle\}$ for the axial motion. For transitions from $F = 3, m = 0$ to $F = 4, m = 0$ and to first order in η, the Rabi frequency for an $n \to n$ transition is $\Omega_{n \to n} = (1/2)(1 + \cos 2\alpha)\,\Omega_0$, while for an $n \to n-1$ transition, it is $\Omega_{n \to n-1} = \eta\sqrt{n}\sin 2\alpha\,\Omega_0$ (similar results hold for other Zeeman sublevels [31]); here, $\eta = (2\pi/\lambda_R)z_0 = 0.056$ is the Lamb-Dicke parameter for axial motion, and $z_0 = \sqrt{\hbar/2m\omega_a} = 8.5$ nm is the ground state wavepacket size. Note that the $n \to n - 1$ transition is strongest for atoms with $\alpha = \pi/4$.

The spatial dependence of the Raman coupling, together with the fact that the the axial motion of the atom is in the Lamb-Dicke limit, allows us to implement Raman sideband cooling [25]. We tune the Raman pair to the red axial sideband ($\delta_R = -525$ kHz $\simeq -\omega_a$) [32] and apply the Ω_4 lattice beams. An atom that starts in $F = 3$ is coherently transferred by $\Omega_{R1,R2}$ to $F = 4$, where it is incoherently repumped to $F = 3$ by Ω_4. The coherent transfer lowers the axial vibrational quantum number n by one, while the incoherent repumping usually leaves n unchanged since n-changing transitions are Lamb-Dicke suppressed. Thus, the beams continually lower n, cooling the atom to the axial ground state. Also, the Ω_4 light provides Sisyphus cooling [27] in the radial direction.

Strong atom-cavity coupling enables a versatile detection scheme for determining if an atom is present in the cavity, and if so, if it is in the $F = 3$ or $F = 4$ manifold. For the current settings, in 100 μs we measure the atomic hyperfine state with a confidence level of $> 98\%$. The scheme involves driving the cavity with a 100 μs pulse of resonant $F = 4 \to F' = 5'$ linearly polarized probe light $\mathcal{E}_P$. As shown in Fig. 2, if an $F = 3$ atom is

present (or if the cavity is empty) then the light is transmitted, while if an $F = 4$ atom is present then the light is blocked because of the strong atom-cavity coupling [9]. Suppose we set the $\mathcal{E}_P$ intensity such that on average N_e photons are detected [33] per probing interval when no atom is in the cavity. Then if the number N of detected photons is such that $N < 0.25 N_e$, we assume an $F = 4$ atom is present, if $N > 0.75 N_e$ we assume an $F = 4$ atom is not present, otherwise the measurement is inconclusive (which happens $< 2\%$ of the time) and we ignore the result. Whenever we detect the atomic state we perform two such measurements: the first with just $\mathcal{E}_P$ to find out if an $F = 4$ atom is present; the second with the $\mathcal{E}_P$ probe together with Ω_3 as a repumper [28], to see if an atom is present at all, regardless of its internal state.

We measure the Raman transfer probability P_4 for a given δ_R by preparing an atom in $F = 3$, applying a Raman pulse, and then detecting the atomic state using the above scheme (with $N_e \sim 22$). We call one such measurement cycle a trial. For each trial, we first Raman-sideband cool the atom for an interval Δt_c. Next, we pump it into $F = 3$ by alternating 1 μs pulses of Ω_4 lattice light with 1 μs pulses of Ω'_4 linearly polarized resonant $F = 4 \rightarrow F' = 4'$ light from the side of the cavity (10 pulses of each). After the atom is pumped to $F = 3$, we apply a $\Delta t_R = 500$ μs Raman pulse, which sometimes transfers it to $F = 4$. Finally, we measure the atomic state and check if the atom is still present. For each atom, we fix the absolute value of the Raman detuning $|\delta_R|$, and alternate trials at $+|\delta_R|$ with trials at $-|\delta_R|$ (299 trials each). By combining data from atoms with different values of $|\delta_R|$, we map out a Raman spectrum. Note that because the initial Zeeman state of the atom is random, all allowed $F = 3 \rightarrow F = 4$ Zeeman transitions contribute to these spectra.

Two example Raman spectra are plotted in Fig. 3. For the (a) curve, we cool for $\Delta t_c = 250$ μs, for the (b) curve for $\Delta t_c = 5$ ms. These scans are performed after nulling the magnetic field to within ~ 40 mG; the widths of the peaks are set by the splitting of different Zeeman levels due to the residual magnetic field. For the curve in panel (a), we see peaks at the carrier ($\delta_R = 0$), as well as at the blue/red sidebands ($\delta_R/2\pi \simeq \pm 530$ kHz $= \pm\omega_a$). Already we note a sideband asymmetry, indicating that a significant fraction of the population is in the $n = 0$ vibrational state. For the (b) data, the red sideband at $\delta_R/2\pi \simeq -530$ kHz is suppressed to such a degree that it cannot be distinguished from the background and contribution from off-resonant excitation of the carrier.

The ratio r of transfer probabilities for the red and blue sideband gives information about the temperature of the atom. For a two-state atom in a thermal state, this ratio r_0 at $|\delta_R| = \omega_a$ is related to the mean vibrational quantum number $\bar{n}$ by $r_0 = \bar{n}/(\bar{n} + 1)$ [25]. In Fig. 3c, we plot r as a function of $|\delta_R|$ for the $\Delta t_c = 5$ ms data. As shown in Fig. 3b, we fit a Lorentzian curve to the carrier, then subtract its contribution from both the red and the blue sideband data, with the result shown in
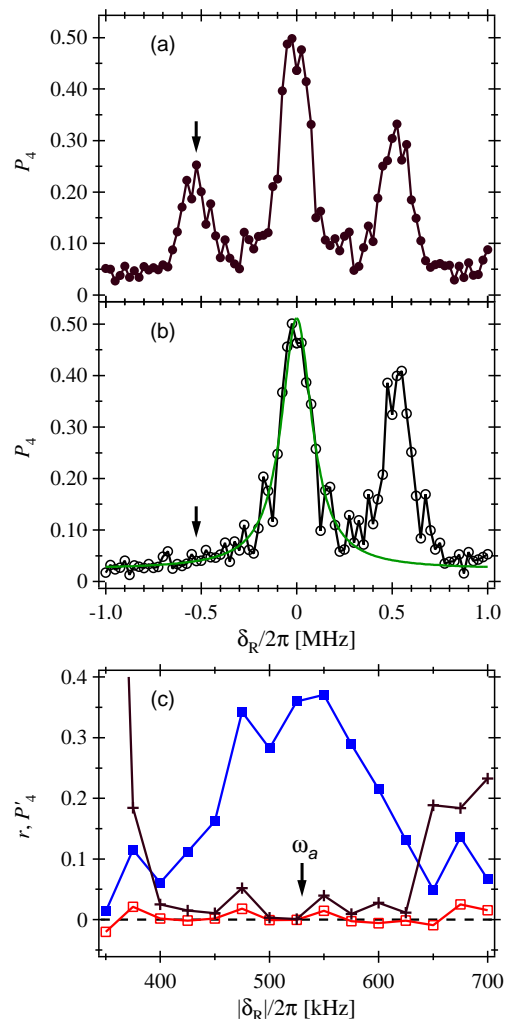

FIG. 3: Population P_4 in the $F = 4$ state versus Raman detuning $\delta_R/2\pi$. The (a) data are taken with $\Delta t_c = 250$ μs of cooling, and with an Ω_4 total 4-beam intensity $I_4 = 5 I_4^{\text{sat}}$; the (b) data with $\Delta t_c = 5$ ms of cooling, and $I_4 = 0.5 I_4^{\text{sat}}$ (on average, about 33 atoms per data point). The arrow marks the detuning used for sideband cooling. (c) Zoom-in on the two sideband regions for the (b) data, with detuning axis folded around $\delta_R = 0$. The red ($\square$) and blue ($\blacksquare$) sidebands, as well as their ratio r (+), are shown after subtracting a Lorentzian fit to the carrier (green curve in (b)).

panel (c). We find $r_0 \simeq \bar{n} = 0.01 \pm 0.05$, and the ground state population $P_0 = 1/(\bar{n} + 1) = 0.99 \pm 0.05$, where the error bars reflect fluctuations in the data around $|\delta_R| = \omega_a$. If instead we subtract the constant background of $P_4^B = 0.024$ but not the carrier's Lorentzian tail, we find $r_0 \simeq \bar{n} = 0.05 \pm 0.04$, and $P_0 = 0.95 \pm 0.04$. Finally, if we use the raw data from Fig. 3b with no subtractions, we obtain $r_0 = 0.10 \pm 0.03$, $\bar{n} = 0.12 \pm 0.04$ and $P_0 = 0.89 \pm 0.03$. Note, however, that because the atom is not a two-state system and the motional state is not known to be thermal, these estimates are approximate.

The axial cooling rate and asymptotic value of $\bar{n}$ depend on δ_R, on the $\Omega_{R1,R2}$ Rabi frequencies, and on the
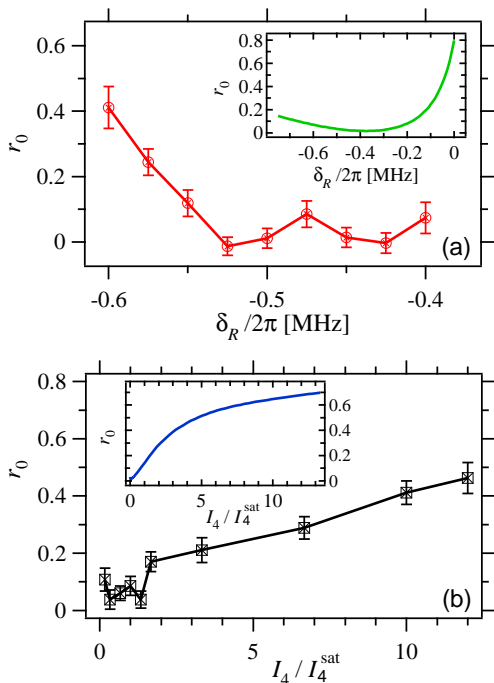
FIG. 4: Varying cooling parameters. The sideband ratio r_0 is shown as a function of (a) the Raman detuning δ_R employed for cooling and (b) the $4 \to 3$ repumping intensity I_4 [34]. Insets show the results from a simple calculation for a 2-state atom trapped in a FORT well with $\alpha = \pi/4$.

power and detuning of Ω_4. We have performed detailed computer simulations to help us choose optimal values for these parameters [31]. A common feature of both our theoretical and experimental investigations is the remarkable robustness of $\bar{n}$ under variations of the cooling parameters. As an example [34], in Fig. 4 we plot the measured sideband ratio r_0 at $\delta_R/2\pi = -500$ kHz $\simeq -\omega_a$ as a function of (a) the detuning δ_R used for sideband cooling, and (b) the recycling intensity I_4. The sideband asymmetry is maintained over a range of at least 200 kHz in detuning, and of two orders of magnitude in the intensity I_4 of the Ω_4 beams. The insets give results from a simple 2-state calculation of r_0, displaying similar insensitivity to the exact values of δ_R and I_4 used for Raman

sideband cooling [31].

As for the radial temperature, we do not yet have an accurate thermometer. We can, however, adiabatically ramp down the FORT depth to zero, so that only the U_R trapping potential remains, and measure the probability that the atom survives the ramping process [35]. Assuming three-dimensional thermal equilibrium (which might not hold for our system), these data limit the temperature to ~ 100 μK. However, the Sisyphus cooling we use radially has been previously shown to reach temperatures of ~ 1 μK [27].

Another way to investigate the efficacy of the cooling is to examine its impact on the lifetime of the atom in the trap. In the presence of state- and atom-detection probing trials, the atomic lifetime is 0.4 s with no cooling, 1.8 s with 250 μs of cooling (settings as in Fig. 3a), and 4.6 s with 5 ms of cooling per trial (as in Fig. 3b).

The Raman coupling provides a versatile tool for cavity QED with trapped atoms beyond cooling the atomic motion that we have focused on here. For example, we have used Raman spectroscopy to null the magnetic field at the trapping sites to ~ 10 mG (including any FORT pseudo-field), to prepare coherent superpositions of two ground states, and to measure the population distribution among Zeeman sublevels for various protocols [36].

In conclusion, we have demonstrated cooling to the ground state of axial motion for single Cesium atoms strongly coupled to the field of a small optical resonator. Together with existing capabilities for strong coupling of the internal degrees of freedom, control over the external center-of-mass motion in cavity QED enables a new set of phenomena to be explored at the light-matter interface. For example, arbitrary states of atomic motion can be prepared from the ground state by coherent Raman transitions [25], then mapped to the electromagnetic field by way of the strong atom-field coupling [24]. Investigations of sensing atomic motion at the standard quantum limit and feedback control now become feasible [18, 37].

[1] T. Pellizzari et al., Phys. Rev. Lett. 75, 3788 (1995).
[2] L.-M. Duan et al., Phys. Rev. Lett. 92, 127902 (2004).
[3] J. I. Cirac et al., Phys. Rev. Lett. 78, 3221 (1997).
[4] H.-J. Briegel et al., in The Physics of Quantum Information, edited by D. Bouwmeester et al., p. 192.
[5] J. Ye et al., Phys. Rev. Lett. 83, 4987 (1999).
[6] J. McKeever et al., Phys. Rev. Lett. 90, 133602 (2003).
[7] P. Maunz et al., Nature 428, 50 (2004).
[8] J. A. Sauer et al., Phys. Rev. A 69, 051804(R) (2004).
[9] A. Boca et al., Phys. Rev. Lett. 93, 233603 (2004).
[10] S. Nußmann et al., Nature Physics 1, 122 (2005).
[11] R. Miller et al., J. Phys. B 38, S551 (2005).
[12] G. R. Guthöhrlein et al., Nature 414, 49 (2001); A. B. Mundt et al., Phys. Rev. Lett. 89, 103001 (2002).
[13] For example: inferred atomic localization ~ 33 nm along and ~ 5.5 μm transverse to the cavity axis [9]; or, positioning of one atom with 135 nm repeatability [14].
[14] S. Nußmann et al., Phys. Rev. Lett. 95, 173602 (2005).
[15] B. G. Englert et al., Europhys. Lett. 14, 25 (1991).
[16] S. Haroche et al., Europhys. Lett. 14, 19 (1991).
[17] M. J. Holland et al., Phys. Rev. Lett. 67, 1716 (1991).
[18] P. Storey et al., Phys. Rev. Lett. 68, 472 (1992); R. Quadt et al., Phys. Rev. Lett. 74, 351 (1995).
[19] A. M. Herkommer et al., Phys. Rev. Lett. 69, 3298

(1992); A. M. Herkommer *et al.*, Quant. Sem. Opt. **8**, 189 (1996).

[20] W. Ren *et al.*, Phys. Rev. A **51**, 752 (1995).

[21] M. O. Scully *et al.*, Phys. Rev. Lett. **76** , 4144 (1996).

[22] D. W. Vernooy and H. J. Kimble, Phys. Rev. A **55** , 1239 (1997); Phys. Rev. A **56**, 4287 (1997).

[23] A. C. Doherty *et al.*, Phys. Rev. A **57**, 4804 (1998).

[24] A. S. Parkins and H. J. Kimble, Journal Opt. B: Quantum Semiclass. Opt. **1**, 496 (1999); *Frontiers of Laser Physics and Quantum Optics,* eds. Z. Xu et al. (Springer, Berlin, 2000), 132; Phys. Rev. A **61**, 052104 (2000).

[25] D. Leibfried *et al.*, Rev. Mod. Phys. **75**, 281 (2003).

[26] S.E. Hamann *et al.*, Phys. Rev. Lett. **80** , 4149 (1998); H. Perrin *et al.*, Europhys. Lett. **42**, 395 (1998); V. Vuletic *et al.*, Phys. Rev. Lett. **81**, 5768 (1998).

[27] D. Boiron *et al.*, Phys. Rev. A **53**, R3734 (1996).

[28] For trap loading, the total power in the four lattice beams is $50I_4^{\mathrm{sat}}$ for Ω_3 and Ω_4, where $I_4^{\mathrm{sat}} \sim 3.8$ mW/cm^2. For atom detection, the Ω_3 intensity is $5I_4^{\mathrm{sat}}$.

[29] Δ'_{HF} for a trapped atom is slightly reduced compared to its free space value $\Delta_{HF} = 9.19263$ GHz, because the FORT potential for the $F = 3$ manifold is slightly weaker than for $F = 4$. For our FORT, the correction is $\Delta'_{HF} - \Delta_{HF} = -21$ kHz [36].

[30] Here Ω_0 is the Rabi frequency for the transition $F = 3, m = 0, n = 0 \rightarrow F = 4, m = 0, n = 0$, where the quantization axis is along the cavity axis.

[31] A. D. Boozer, in preparation.

[32] Note that for $\delta_R = -\omega_a$, an $F = 3 \rightarrow F = 4$ ($F = 4 \rightarrow F = 3$) Raman transition lowers (raises) n by one.

[33] The probability for a photon starting out within the cavity to be recorded by our detectors is $e \sim 0.06$.

[34] Unless otherwise noted, the settings for this measurement are: $I_4 = 0.3I_4^{\mathrm{sat}}$, $\Delta t_c = 5$ ms, $\delta_R = -500$ kHz, $\Delta t_R = 50$ μs; $P_4^B = 0.065$ was subtracted before computing r_0.

[35] W. Alt *et al.*, Phys. Rev. A **67**, 033403 (2003).

[36] A. D. Boozer, PhD thesis (2005), http://etd.caltech.edu.

[37] A. Doherty and K. Jacobs, Phys. Rev. A **60**, 2700 (1999).